A New and Simple Mathematical Technique to Study the Steady-state Performance of Isolated Asynchronous Generator

Himadri Sekhar Chatterjee* and Sankar Narayan Mahato

Department of Electrical Engineering, National Institute of Technology, Durgapur-713209, West-Bengal, India
E-mail: chatterjeehimadri91@gmail.com; snmrec@yahoo.co.in
**Corresponding Author*

Received 27 July 2021; Accepted 20 November 2021;
Publication 16 February 2022

Abstract

Isolated Asynchronous Generator (IAG) is nowadays widely used for renewable power generation from the sources like wind and small hydro. Traditionally, the steady-state analysis of IAG is carried out by solving a complex higher order non-linear polynomial equation obtained in a complicated way from the steady-state circuit diagram. In this paper, a simple new mathematical procedure has been introduced to obtain two non-linear polynomial equations in much more simplified form which can easily be solved for the unknown variables i.e., per unit generated frequency (a) and magnetizing reactance (X_m). Between these two equations, one equation comprises only one unknown variable'a' and hence, easy to solve. Differential Search Algorithm (DSA) has been efficiently implemented for solving these non-linear equations. The computational efficacy of DSA has been compared with that of Newton-Raphson (N-R) method, Linear Search Algorithm (LSA), Binary Search Algorithm (BSA) and Particle Swarm Optimization (PSO)

Distributed Generation & Alternative Energy Journal, Vol. 37_3, 663–682.
doi: 10.13052/dgaej2156-3306.37313

technique. The performance of the IAG has been studied under different operating conditions such as variation of speed, capacitance and load. All the simulated results have been experimentally verified using a three-phase, 415 volts, 2.2 kW, star-connected induction generator and a close agreement has been found.

Keywords: BSA, DSA, isolated asynchronous generator, LSA, performance analysis, PSO.

Nomenclature: a-per unit generated frequency; b-per unit speed; C-per-phase shunt capacitance; E_g-per phase generated air gap voltage; Ic-per phase capacitor current; I_L-per phase load current; I_R-per phase rotor current; I_S-per phase stator current; P_O-per phase output power; P_Q-per phase reactive power generated; R_1, R_2-stator and rotor (referred to stator) resistance per phase respectively; X_1, X_2-stator and rotor (referred to stator) leakage reactances per phase respectively; V_L-per-phase load terminal voltage; X_m-per-phase magnetizing reactance; R_L, X_L-per phase load resistance and reactance respectively.

1 Introduction

Electrification of rural areas, situated in remote locations, is an important task that should be carried out by any developing nation for its sustainable development. It has been found that these remote areas are glorified with sustainable energy sources like biomass, solar, wind, small hydro, etc. An economical and feasible solution for supplying power to these remote areas is, therefore, to develop small-scale power generating systems using these renewable energy sources. An Isolated Asynchronous Generator (IAG), due to its own merits such as low unit cost, rugged construction, little maintenance and most importantly its inherent short-circuit protection against faults, can efficiently be used in such systems for generating power from small hydro and wind.

With a proper capacitor bank fixed over the stator terminals of the IAG, if its rotor is made to rotate at a speed above some critical value, the generator initiates voltage build-up and sequentially power may be supplied to the consumer loads. The schematic diagram of a three-phase IAG supplying three-phase load has been shown in Figure 1. The performance of IAG depends mainly on prime mover speed, excitation capacitance and load. The performance analysis of IAG at steady-state is carried out from its per-phase

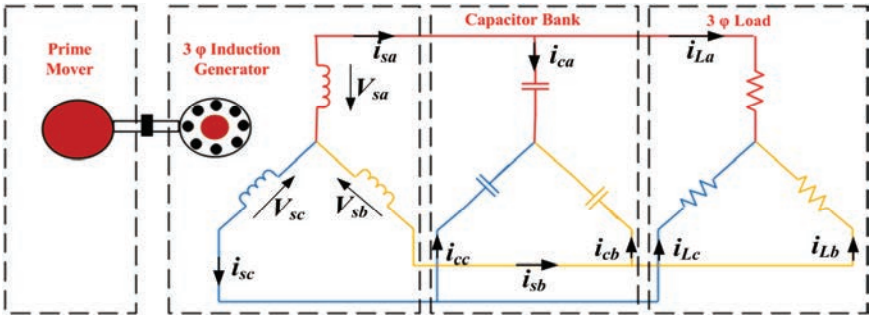

Figure 1 Schematic diagram of three-phase IAG feeding three-phase load.

equivalent circuit. Quazene and McPherson [1] have used nodal admittance method whilst Malik and Haque [2] have suggested loop impedance technique to solve the equivalent circuit. Modelling of IAG using a two-port network and its steady-state performance, have been reported by Wang and Huang [10] and Ray et al. [28]. Haque [13] has proposed a P-Q load model of IAG for analysis while design based computational procedure has been suggested by Murthy et al. [19]. Control-oriented linearized state-space model has been presented by Kiselychnyk et al. [23].

For carrying out the study of IAG, two higher order complex equations comprising of two variables 'X_m' and 'a' are obtained from the equivalent circuit of IAG. Solutions to these equations are primarily done by iterative method [3] and Newton-Raphson method [4]. Alolah and Alkanhal [5] have used classic gradient optimizers for minimization of the cost function of either the total admittance or impedance of the generator. Pattern Search method of Hooke and Jeeves has been applied for function minimization [6] while Simulated Annealing (SA) [7, 12] technique has been used for voltage regulation optimization problem. Genetic algorithm (GA) based method of solving the optimization problem of three-phase IAG connected to three-phase load [9], single-phase load [8], battery charging application [14], dc load [20] and another three-phase induction generator operating in parallel [26] have also been reported. Haque [11] has used numerical based "fsolve" to solve the unknown variables. Bjornstedt et al. [15] have proposed an algorithm for easy interpretation of loading effects on the characteristic behaviour of IAG.

The higher order equations developed while solving the equivalent circuit have been reduced using Graph Theory based approach [21, 22]. Ibrhahim and Serag [16] have used Particle Swarm Optimization for solution of

the objective function for normal shunt excited induction generator while Chauhan et al. [18] have successfully implemented the said algorithm for short-shunt induction generator. A number of well known algorithms namely Direct Algorithm [17], Linear Search Algorithm (LSA) [24], Binary Search Algorithm (BSA) [24, 28], Cuckoo Search Algorithm [25] and Taguchi Optimization (TM) method [27] have been employed successfully to solve the equations. Ray et al. [28] have used BSA algorithm for solution of the complex non-linear equations but have restricted its analysis to machine operating under constant speed and feeding resistive load. The present paper have included the various factors like loadability, speed and capacitance value and its corresponding impact on the performance of the IAG. Most importantly, the added advantage of the present work over other available techniques is that the proposed method has reduced the complex mathematical deduction of the equations into a simple one, as well as, the equation contains only one unknown variable and hence easy to solve. From the literature, it is found that the derivation and also the solution of the two non-linear equations, which are essential for studying the steady-state behaviour of the IAG, are very complex. Accordingly, the main contributions of this paper includes –

(i) Development of a new and simple mathematical procedure that reduces the lengthy mathematical derivations of these two nonlinear equations.
(ii) One of these two equations obtained using this new approach has only one unknown variable and hence, it is easy to solve.
(iii) Moreover, DSA has been efficiently implemented for solving the variables 'X_m' and 'a'.
(iv) The computational efficiency of DSA has been compared with N-R method, LSA, BSA, PSO technique.
(v) The steady-state behaviour of the IAG has been investigated using DSA under various operating conditions such as variations in load, capacitance and speed.
(vi) All the simulated results have been validated experimentally.

This paper has been organized into five sections. Section-1 includes the main advantages of three-phase IAG over conventional synchronous generator and a brief literature review on the steady-state analysis of IAG under various operating conditions. In Section-2, the proposed simple mathematical model of the system has been presented. Section-3 discusses the application of Differential Search Algorithm in solving the proposed mathematical model equations. The computational efficiency of DSA has been compared with other algorithms in Section-4. Also the steady-state analysis of the generator

operating at various conditions has been presented in this section. Section-5 shows the conclusions drawn from this study.

2 Problem Formulation

Three-phase IAG and its corresponding per phase steady-state circuit have been represented in Figure 2. All the previous researchers have employed either loop impedance or nodal admittance method [1, 2] for solving the equivalent circuit. In these methods, complex and lengthy mathematical derivations are required for obtaining two higher order non-linear equations containing the two unknown parameters which are required to be solved. Moreover, the solutions of these two non-linear equations are also complicated.

The proposed new method is presented below:

From Figure 2, it can be written as:

$$\text{Load impedance, } Z_L = \frac{R_L}{a} + jX_L \tag{1}$$

$$\text{Capacitive reactance, } Z_C = -j\frac{X_C}{a^2} \tag{2}$$

$$\text{Stator impedance, } Z_S = \frac{R_1}{a} + jX_1 \tag{3}$$

$$\text{Rotor impedance, } Z_R = \frac{R_2}{a-b} + jX_2 \tag{4}$$

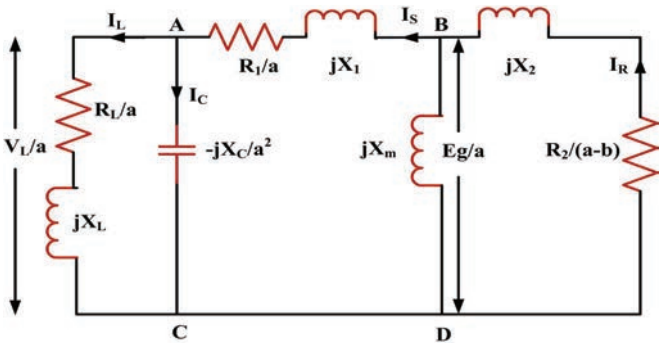

Figure 2 Steady-State Circuit diagram of IAG.

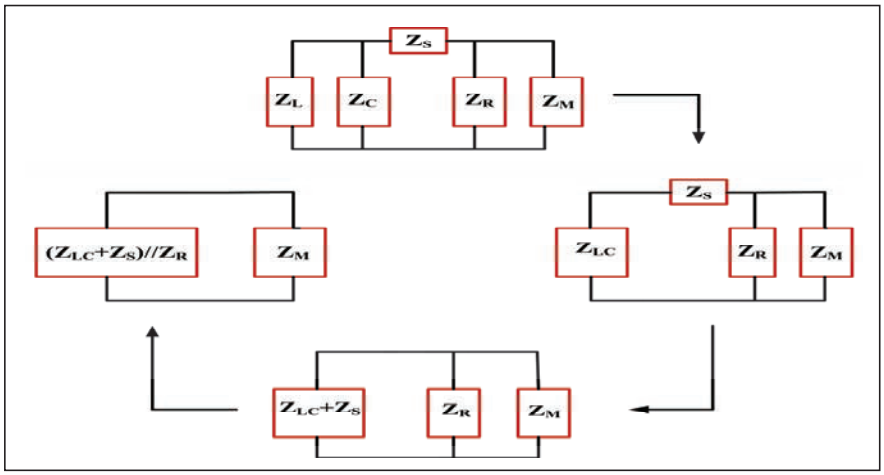

Figure 3 Reduced Equivalent Diagram of IAG.

The reduced equivalent diagram of Figure 2 is shown in Figure 3. The net impedance of this circuit must be zero and can be written as:

$$Z_{SR} + Z_M = 0 \tag{5}$$

where,

$$\frac{1}{Z_{SR}} = \frac{1}{Z_S + \frac{Z_L * Z_C}{Z_L + Z_C}} + \frac{1}{Z_R};$$

and

$$Z_M = jX_m$$

Putting the values of Z_m, the final equation becomes

$$\frac{1}{Z_{SR}} = \frac{j}{X_M} \tag{6}$$

Breaking up Equation (6) into real and imaginary sections yields

$$real\left(\frac{1}{Z_{SR}}\right) = 0 \tag{7}$$

$$imag\left(\frac{1}{Z_{SR}}\right) = \left(\frac{1}{X_m}\right) \tag{8}$$

It is found that 'a' is the sole variable present in Equation (7). Resolving Equation (7) for 'a' and putting its corresponding value in Equation (8), the

other unknown variable 'X_m' is solved. Therefore, the proposed method is very simple and the complex, lengthy derivation can be avoided. Moreover, as Equation (7) contains only one variable 'a', the solution of this equation is also easy.

After solving for 'X_m', from the magnetization characteristics of the generator,(Eg/a) is determined corresponding to the value of 'X_m'. With the known values of (Eg/a), X_m,a, X_C, b, R_L, R_1, R_2; the current flowing throughout the load, capacitor, stator and rotor can be found out with the help of circuit diagram presented in Figure 2. Accordingly, the load terminal voltage, reactive power and output power consumed may be determined.

1. $$\mathrm{I_S} = \frac{\frac{\mathrm{E_g}}{\mathrm{a}}}{\left(\frac{\mathrm{R_1}}{\mathrm{a}} + \mathrm{jX_1}\right) + \left(\frac{\mathrm{R_L}}{\mathrm{a}} + \mathrm{jX_L}\right) // \left(-\mathrm{j}\frac{\mathrm{X_C}}{\mathrm{a^2}}\right)} \tag{9}$$

2. $$\mathrm{I_R} = \frac{-\frac{\mathrm{E_g}}{\mathrm{a}}}{\frac{\mathrm{R_2}}{\mathrm{a-b}} + \mathrm{jX_2}} \tag{10}$$

3. $$\mathrm{I_L} = \mathrm{I_S}\frac{\left(-\mathrm{j}\frac{\mathrm{X_C}}{\mathrm{a^2}}\right)}{\left(\frac{\mathrm{R_L}}{\mathrm{a}} + \mathrm{jX_L}\right) + \left(-\mathrm{j}\frac{\mathrm{X_C}}{\mathrm{a^2}}\right)} \tag{11}$$

4. $$\mathrm{I_C} = \mathrm{I_S} - \mathrm{I_L} \tag{12}$$

5. $$\mathrm{V_L} = \mathrm{aI_L}\left(\frac{\mathrm{R_L}}{\mathrm{a}} + \mathrm{jX_L}\right) \tag{13}$$

6. $$\mathrm{P_O} = \mathrm{I_L^2}\left(\frac{\mathrm{R_L}}{\mathrm{a}} + \mathrm{jX_L}\right) \tag{14}$$

7. $$\mathrm{P_Q} = \mathrm{I_C^2}\,\frac{\mathrm{X_C}}{\mathrm{a}} \tag{15}$$

Figure 4 demonstrates the deviation of $real(\frac{1}{Z_{SR}})$ with variation in 'a'. From the figure a conclusion may be drawn that for a particular value of 'a', $real(\frac{1}{Z_{SR}})$ will be zero. Variations in frequency ranging from 0.5 p.u. to 1.5 p.u. at different speeds have been used to plot the curve in Figure 4. Additionally, 160Ω load resistance and 35 μF shunt capacitance has been considered for Figure 4. The selection of capacitance value is made based on the transient analysis of IAG under no-load condition. It has been observed that for 35 μF, the machine generates the rated no-load voltage of 240 V (phase voltage).

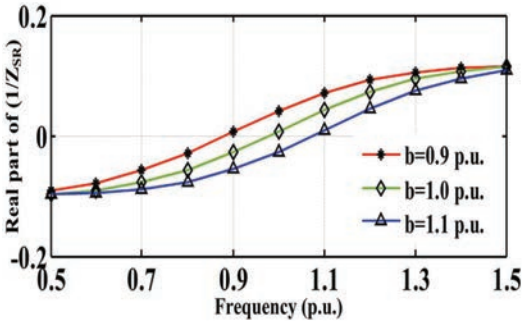

Figure 4 Deviation of $real(1/Z_{SR})$ with frequency variation.

3 Differential Search Algorithm

Civicioglu [29] developed Differential Search Algorithm (DSA) to solve various optimization problems. The algorithm replicates the Brownian-like-random-walk movement used by an individual to move about. The major advantage of DSA over classical algorithms is its ability to avoid local optimal solutions. Other advantages includes (i) less number of iterations to reach the best fitness value, (ii) low tolerance value, (iii) low computational time.

The detailed working of the algorithm in solving the optimized problem has been shown in Figure 5. Every person of $artificialorganism[P(a,b)]$ is initialized by

$$P_{(a,b)} = Low_b + rand * (Up_b - Low_b) \tag{16}$$

where, Up_b and Low_b are the upper and lower boundary limits of the organization respectively, $rand$ represents the arbitrary number between 0 and 1.

The stopover site equation is

$$stopoversite = superorganism + scale * (donor - superorganism) \tag{17}$$

The scale is evaluated by

$$scale = rand_g * (2 * rand1) * (rand2 - rand3) \tag{18}$$

where, $rand1$, $rand2$, $rand3$ correspond to the arbitrary numbers between 0 and 1 by means of uniform distribution and $rand_g$ corresponds to the arbitrary number between 0 and 1 selected by using gamma distribution.

$Artificialorganism$ is being substituted by $stopoversite$ subject to the condition of better effective results obtained from the former. The algorithm ceases to operate once the system reaches its global least point.

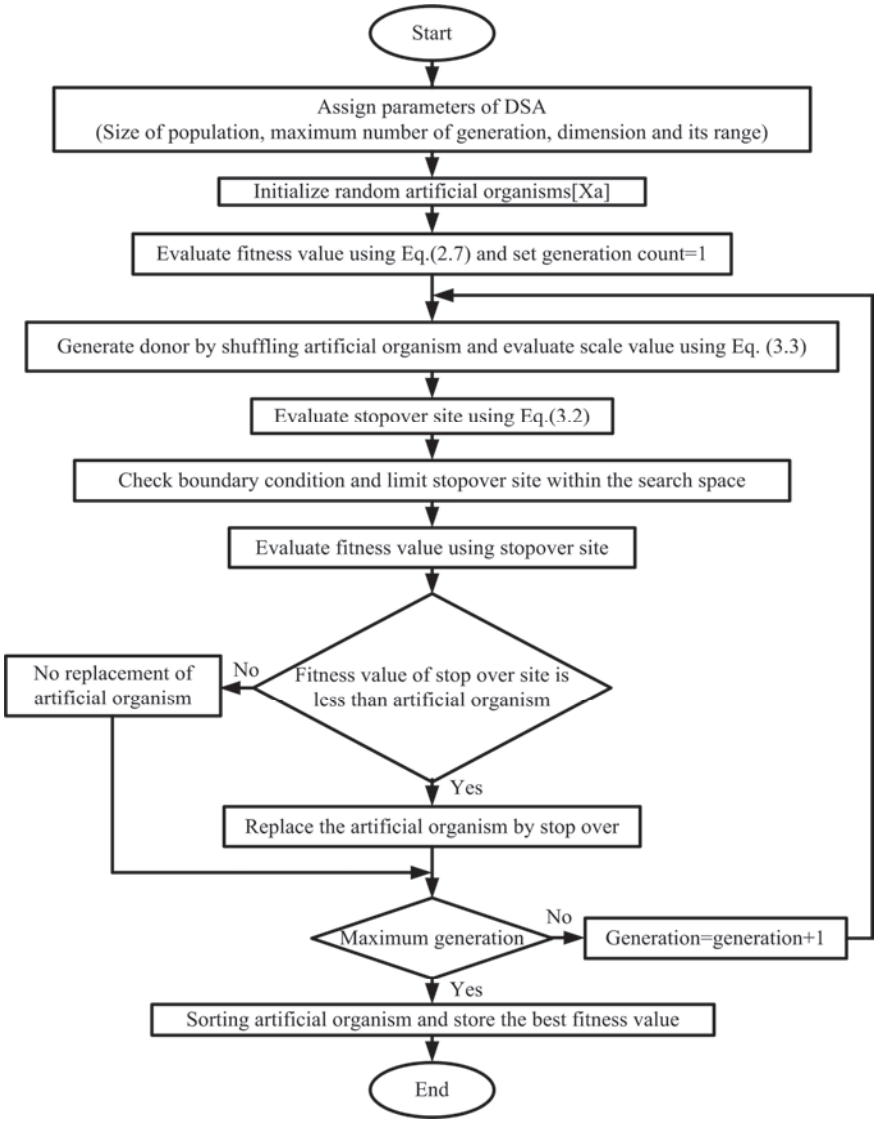

Figure 5 Flowchart of DSA.

4 Results and Discussions

The machine utilized throughout the experiment as well as simulation is a $three - phase$, $star - connected$, $squirrel\ cage$, 2.2 kW, 415 V, 4.61 A,

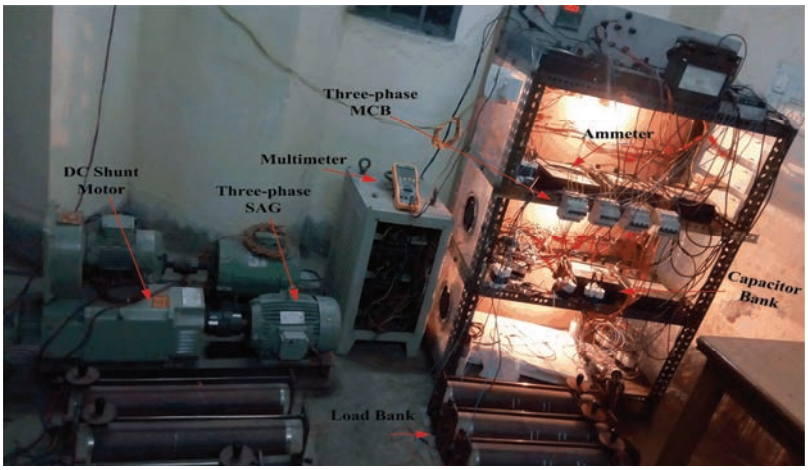

Figure 6 Test bench arrangement of IAG.

4-*pole* induction machine with per phase equivalent circuit parameters: $R_1 = 3.71\Omega$, $R_2 = 2.846\Omega$, $X_1 = 4.98\Omega$, $X_2 = 4.98\Omega$. The magnetization curve of the machine as obtained by experimentation is given below:

$$\begin{cases} E_g = 249.1 & \text{for } X_m < 76.5 \\ \quad = 0.000229{X_m}^3 - 0.104{X_m}^2 & \text{for } 76.5 < X_m < 141.65 \\ \qquad +11.6X_m - 134 & \\ \quad = 0 & \text{for } X_m > 141.65 \end{cases} \tag{19}$$

A test bench has been developed in the laboratory to validate the simulated results. The arrangement consists of an induction generator coupled with a dc shunt motor administering as the prime mover, measuring devices, load bank and set of capacitors with different capacitance values. Three-phase, four-pole Miniature Circuit Breaker (MCB) is used to switch the capacitor bank across the stator terminals of IAG at no-load and loaded conditions. A detailed view of the arrangement has been depicted in Figure 6.

4.1 Comparison of Computational Efficiency

Figure 7 demonstrates the deviation of frequency generated with the change in load resistance, by employing different optimization techniques with per phase capacitance value of 35 μF when the generator is guided at a speed of 1500 rpm and the results are compared with the test results. It has been

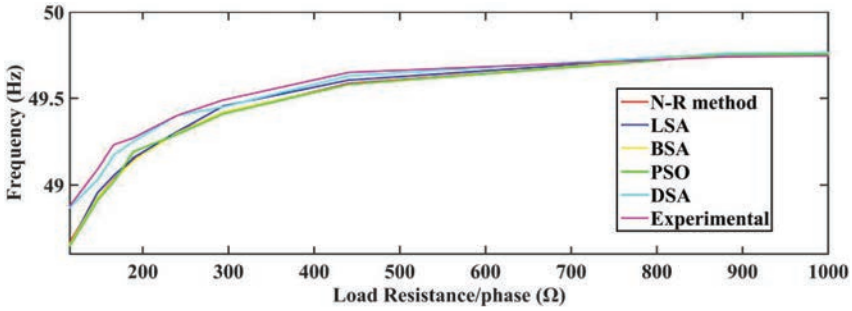

Figure 7 Variation of frequency with change in load resistance.

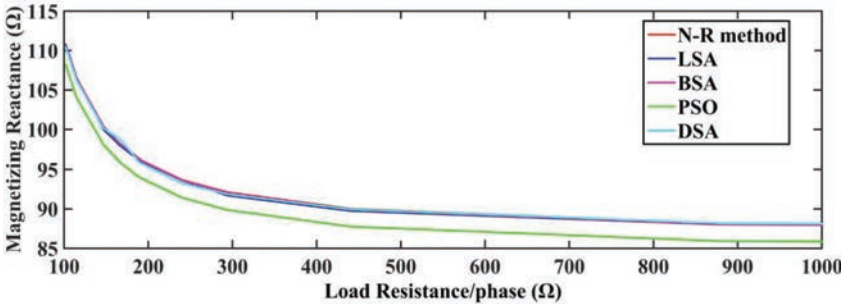

Figure 8 Variation of magnetizing reactance with change in load resistance.

noted that the simulated and the experimental results are compact with one another. A gradual increase in the load demand (i.e., decrease in load resistance) progressively reduces the frequency of the generated voltage when the machine runs at a fixed speed and capacitance. Also, the change in magnetizing reactance with variation in load, with the rotor speed kept fixed at 1500 rpm, has been shown in Figure 8. A quite closeness of the results is observed.

The convergence of fitness function with respect to the number of iterations using DSA has been shown in Figure 9. It is clear from the figure that the objective function takes around 8 iterations to converge to its respective value with a tolerance value of 4.5491e-6. The objective function shown in Figure 9 has been tested at a speed of 1500 rpm with capacitance value of 35 μF per phase at no-load condition. The final per unit frequency at this operating point is 0.9986.

Table 1 compares the computational efficiency i.e., computational time and number of iterations taken to execute the function for different algorithms

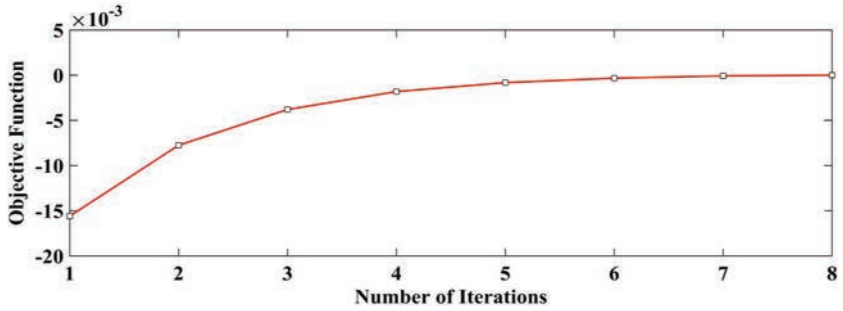

Figure 9 Convergence of DSA algorithm with number of iterations.

Table 1 Comparison of computational efficiency of different algorithms

Load Resistance/ Phase (Ω)	No of Iterations					Computational Time (Sec)				
	N-R Method	LSA	BSA	PSO	DSA	N-R Method	LSA	BSA	PSO	DSA
5000	12	91	8	7	6	3.1625	0.3496	0.3379	0.2564	0.0138
189	15	75	7	9	7	2.3585	0.3459	0.3122	0.4457	0.0581
147	11	71	9	9	7	2.2712	0.3389	0.4156	0.4220	0.0592
115	14	65	9	7	2	2.1201	0.3368	0.3378	0.3681	0.0531
102	12	62	7	7	5	2.0740	0.3233	0.4085	0.3846	0.0618

that includes N-R method, PSO, LSA, BSA and DSA. In all the instances, DSA has presented an enhanced performance with respect to other algorithms. For this reason, the detailed steady-state analysis of the IAG has been carried out using DSA.

4.2 Performance of IAG at 0.8 p.f. Lagging Load

In this part, the main focus is to analyze the performance of IAG operating at constant speed and varying inductive load. With constant capacitance excitation and speed, the value of the frequency is decreased with an increase in load demand (Figure 10(a)). The variation of load terminal voltage with increase in load power is shown in Figure 10(b). As the load demand increases, the terminal voltage reduces until a threshold point is reached, beyond which the output power also decreases along with the voltage irrespective of the load demand. The fixed capacitor bank lacks the ability to supply the additional reactive power demand by the additional inductive load and hence the terminal voltage reduces with the increase in output power. The load current also rises upto a certain point and then again reduces irrespective of the load demand as shown in Figure 10(c). The deviation in stator current

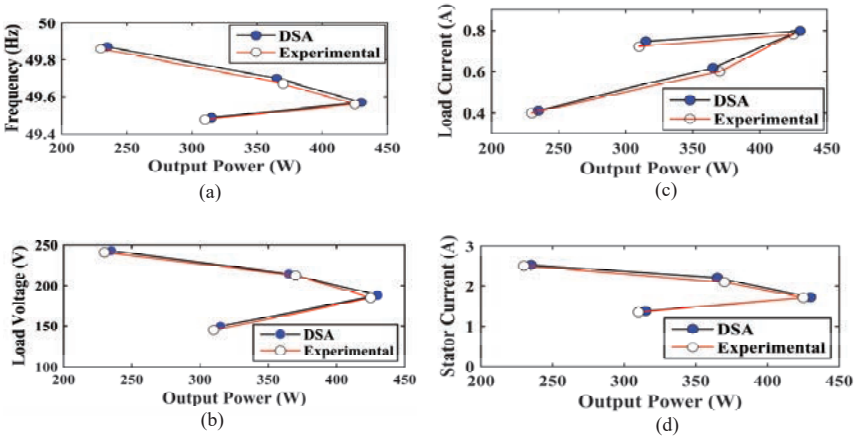

Figure 10 Variations of (a) generated frequency (b) load voltage, (c) load current, (d) stator current with output power at 0.8 lagging p.f. load.

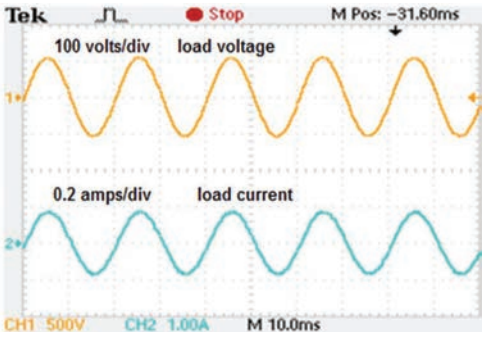

Figure 11 Experimental waveform of load terminal voltage (line to line) and load current at 0.8 lagging p.f. load.

with variation in output power demand has been displayed in Figure 10(d). All the simulated results are in close agreement with the experimental results. The experimental waveform of per phase load voltage (line to line) and load current at steady-state has been shown in Figure 11. In all the above cases, the generator runs at 1500 rpm with shunt capacitance of 35 μF/phase.

4.3 Performance of IAG at Variable Speed and No-load

The purpose of this section is to study the effect of speed variation on the frequency, no-load voltage as well as stator current of the generator under no-load condition. IAGs are installed primarily in the remote and rural areas and

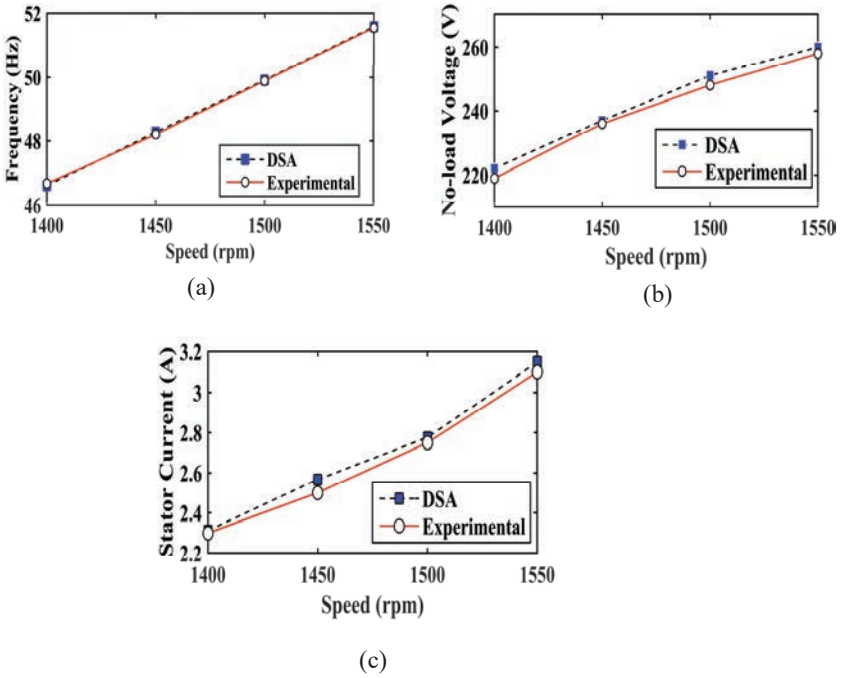

Figure 12 Variation of (a) frequency, (b) load terminal voltage (phase), (c) stator current with speed.

there are instances of switching off the load from time to time. This results in an increased runaway speed of the machine, which results in an increased voltage across the stator terminals. This consecutive increment in the voltage level causes damage to the insulation of the stator coils, which further results in a short circuit between the coils and hence damages the generator.

The no-load behaviour has been tested using a three-phase capacitor bank of 35 μF/phase. For safety purpose of the machine, its voltage is restricted to 1.3 times the rated voltage. The generated frequency is directly proportional to the speed of the machine and as a result, with an increase in speed, the generated frequency increases as shown in Figure 12(a). In addition, an increased speed results in increase of reactive power supplied to the machine, which causes an increase in terminal voltage as well as the stator current as given in Figure 12(b) and Figure 12(c) respectively. Figure 13 shows the experimental waveform of no-load terminal voltage across the stator terminals operating at a speed of 1500 rpm and shunt excitation capacitance of 35 μF/phase.

Figure 13 Phase voltage at 1500 rpm.

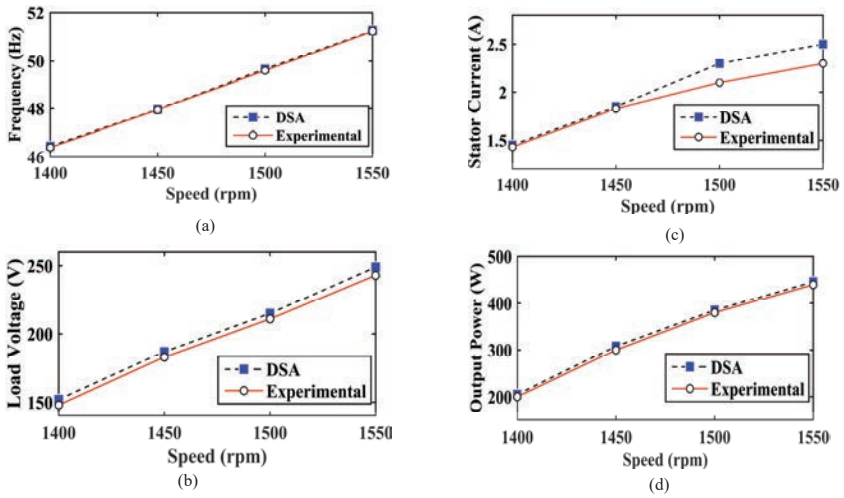

Figure 14 Variation of (a) Frequency, (b) Load voltage, (c) Stator current, (d) Output power at 0.8 p.f. load.

4.4 Performance of IAG at Variable Speed and Load

With an inductive load fixed across the stator terminals of IAG, the reactive power demand increases with the increase in load. The capacitor bank of fixed size connected in parallel with the IAG terminals has a limitation of supplying additional reactive power and as a result, the terminal voltage of the IAG drops. This problem due to the demand of additional reactive power may be partially solved by increasing the speed of IAG. Figure 14(a)–(d) describe the performance of IAG with fixed size capacitor bank of 35 μF/phase

connected across the stator terminals and a constant 0.8 lagging p.f. load with the variation in speed of the machine. The generated frequency of IAG is directly proportional to the speed of the machine. Hence, for a fixed lagging p.f. load, an increased speed of the machine results in an increase in frequency as shown in Figure 14(a). Since, an increased speed reduces the magnetizing requirements of IAG and increases the reactive power produced by the capacitor bank, therefore, this additional VAR requirement of the inductive load is compensated with an increase in speed of the machine. Correspondingly, there is an improvement in voltage across the stator terminals (Figure 14(b)) and also there is an incremental rise in stator current with the increased speed (Figure 14(c)). Moreover, the power output of the generator is directly proportional to the speed. Therefore, with a fixed inductive load, the power output is increased with an increase in speed as given in Figure 14(d).

4.5 Performance of IAG with Variable Capacitance and Load

The IAG suffers from poor voltage regulation with increase in load. This is due to the gap between the VARs demanded by the load and that supplied by the capacitors. Hence, to keep the terminal voltage at constant value with the increase in load, the capacitances are required to be increased. Figure 15(a) shows the requirement of capacitance for maintaining constant terminal voltage with the increase in load. The machine has been kept running at 1500 rpm. The corresponding variation of frequency is given in Figure 15(b). There is a decrease in generated frequency with an increase in load. The reference voltage which is maintained in our study is 240 V (phase voltage).

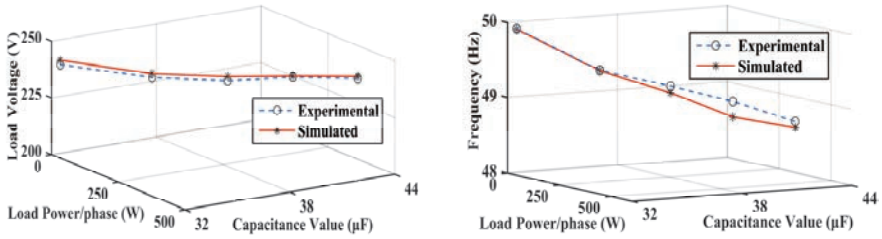

(a) (b)

Figure 15 Variation of (a) load voltage, (b) frequency with load power and capacitance value at a speed of 1500 rpm.

5 Conclusions

A new simple mathematical approach to obtain the non-linear higher orderequations from the per-phase equivalent circuit required to study the steady-state behaviour of three-phase IAG, has been proposed and implemented. DSA has been efficiently used to solve these equations and find the steady-state behaviour of the IAG. The variations of load terminal voltage, stator current, frequency with change in power demand have been thoroughly investigated. Also the effect of the variation of excitation capacitance and speed on the performance of IAG has been presented. The computational efficiency of DSA has been compared with other established algorithms and it is found that DSA gives better performance with minimal computational time and less iterations. All the simulated results have been validated through experimentation. The close conformity between the simulated and the experimental results proves the efficacy of the projected method and algorithm in this paper. Additionally, in the near future, the proposed simple mathematical procedure as well as the algorithm may further be applied for steady-state analysis of IAG operating in parallel with another induction generator and supplying both static and dynamic load.

References

[1] L. Quazene and G. McPherson Jr., 'Analysis of an isolated induction generator', IEEE Trans. Power App. Syst., vol. 102, pp. 2793–2798, 1983.

[2] N. H. Malik and S. E. Haque, 'Steady state analysis and performance of an isolated self excited induction generator', IEEE Trans. Energy Convers., vol. 1, no. 3, pp. 133–139, 1986.

[3] T. F. Chan, 'Analysis of self-excited induction generators using iterative method', IEEE Trans. Energy Convers., vol. 10, pp. 502–507, 1995.

[4] S. S. Murthy, O. P. Malik and A. K. Tandon, 'Analysis of self excited induction generator', Proc. Inst. Elect. Eng. C, vol. 129, pp. 260–265, 1982.

[5] A. L. Alolah and M. A. Alkanhal, 'Optimization-based steady state analysis of three phase self-excited induction generator', IEEE Trans. Energy Convers., vol. 15, no. 1, pp. 61–65, 2000.

[6] T. F. Chan and L. L. Lai, 'Steady-state analysis and performance of a stand-alone three-phase induction generator with asymmetrically connected load impedances and excitation capacitances', IEEE Trans. Energy Convers., vol. 16, no. 4, pp. 327–333, 2001.

[7] S. P. Singh, S. K. Jain and J. Sharma, 'Voltage regulation optimization of compensated self-excited induction generator with dynamic load', IEEE Trans. Energy Convers., vol. 19, no. 4, pp. 724–732, 2004.
[8] N. Kumaresan, 'Analysis and control of three-phase self-excited induction generators supplying single-phase ac and dc loads', Proc. Inst. Elect. Eng.—Elect. Power Appl., vol. 152, no. 3, pp. 739–747, 2005.
[9] D. Joshi, K. S. Sandhu and M. K. Soni, 'Constant voltage constant frequency operation for a self-excited induction generator', IEEE Trans. Energy Convers., vol. 21, no. 1, pp. 228–234, 2006.
[10] Y. J. Wang and Y. S. Huang, 'Analysis of a stand-alone three-phase self excited induction generator with unbalanced loads using a two-port network model', IET Elect. Power Appl., vol. 3, no. 5, pp. 445–452, 2009.
[11] M. H. Haque, 'A Novel Method of Evaluating Performance Characteristics of a Self-Excited Induction Generator', IEEE Trans. Energy Convers., vol. 24, no. 2, pp. 358–365, 2009.
[12] Y. N. Anagreh, 'Performance analysis of self-excited induction generator using simulated annealing algorithm', Int. J. Model Simul., vol. 30, no. 2, pp. 218–222, 2010.
[13] M. H. Haque, 'Analysis of a self-excited induction generator with p–q load model', IEEE Trans. Energy Convers., vol. 25, no. 1, pp. 265–267, 2010.
[14] R. Karthigaivel, N. Kumaresan and M. Subbiah, 'Analysis and control of self-excited induction generator-converter systems for battery charging applications', IET Elect. Power Appl., vol. 5, no. 2, pp. 247–257, 2011.
[15] J. Bjornstedt, F. Sulla and O. Samuelsson, 'Experimental investigation on steady-state and transient performance of a self-excited induction generator', IET Gener. Transm. Distrib., vol. 5, no. 12, pp. 1233–1239, 2011.
[16] H. E. A. Ibrahim and M. F. Serag, 'Analysis of self excited induction generator using particle swarm optimization', World Acad. Sci. Eng. Technol., vol. 5, no. 9, 2011.
[17] A. Kheldoun, L. Refoufi and D. E. Khodja, 'Analysis of theself-excited induction generator steady state performance using a new efficient algorithm', Electr. Power Syst. Res., vol. 86, pp. 61–67, 2012.
[18] Y. K. Chauhan, V. K. Yadav and B. Singh, 'Optimum utilisation of self-excited induction generator', IET Elect. Power Appl., vol. 7, no. 9, pp. 680–692, 2013.

[19] S. S. Murthy, B. Singh and V. Sandeep, 'Design-based computational procedure for performance prediction and analysis of single-phase self-excited induction generator', IET Elect. Power Appl., vol. 7, no. 6, pp. 477–486, 2013.

[20] S. S. Kumar, N. Kumaresan, M. Subbiah and M. Rageeru, 'Modelling, analysis and control of stand-alone self-excited induction generator pulse width modulation rectifier systems feeding constant dc voltage applications', IET Gener. Transm. Distrib., vol. 8, no. 6, pp. 1140–1155, 2014.

[21] S. Ray, S. N. Mahato and N. K. Roy, 'Performance analysis of isolated 3-phase self excited induction generator using graph theory and pso technique', Proc. of IEEE Int. Conf. TENCON, pp. 1–6, 2014.

[22] H. S. Chatterjee and S. N. Mahato, 'Steady-state analysis of isolated three-phase induction generator using adaptive pso technique', Proc. of IEEE Int. Conf. INDICON, pp. 1–5, 2015.

[23] O. Kiselychnyk, M. Bodson and J. Wang, 'Linearized state-space model of a self-excited induction generator suitable for the design of voltage controllers', IEEE Trans. Energy Convers., vol. 30, no. 4, pp. 1310–1320, 2015.

[24] K. Arthishri, K. Anusha, N. Kumaresan and S. S. Kumar, 'Simplified methods for the analysis of self-excited induction generators', IET Electr. Power Appl., vol. 11, pp. 1636–1644, 2017.

[25] H. M. Hasanien and G. M. Hashem, 'A cuckoo search algorithm optimizer for steady-state analysis of self-excited induction generator', Ain Shams Eng. J., vol. 9, no. 4, pp. 2549–2555, 2018.

[26] R. E. Raj, C. Kamalakannan and R. Karthigaivel, 'Genetic algorithm-based analysis of wind-driven parallel operated self-excited induction generators supplying isolated loads', IET Renew. Power Gener., vol. 12, no. 4, pp. 472–483, 2018.

[27] D. Bouhadjra, A. Kheldoun and A. Zemouche, 'Performance analysis of stand-alone six-phase induction generator using heuristic algorithms', Math. Comput. Simulat., vol. 167, pp. 231–249, 2020.

[28] S. Ray, H. S. Chatterjee, D. Samajpati, S. N. Mahato and N. K. Roy, 'Two-port network-based modeling and analysis of three-phase self-excited induction generator used in renewable energy systems', Lect. Notes Electr. Eng., vol. 693, pp. 411–418, 2021.

[29] P. Civicioglu, 'Transforming geocentric cartesian coordinates to geodetic coordinates by using differential search algorithm', Comput. Geosci., vol. 46, no. 15, pp. 229–247, 2012.

Biographies

HimadriSekhar Chatterjee received his B. Tech and M. Tech degrees from Haldia Institute of Technology, Haldia and National Institute of Technology, Durgapur, India, respectively. He is currently pursuing his PhD degree from NIT, Durgapur. His research interest includes renewable energy sources, electrical machines and drives.

Sankar Narayan Mahato is a professor in the department of electrical engineering at National Institute of Technology, Durgapur, India. He received his B.E and M. Tech degree from NIT, Durgapur and PhD degree from Indian Institute of Technology, Roorkee, India. His research interest lies in the field of electrical machines and drives, renewable energy systems, etc.